Earth and Planetary Science Letters 287 (2009) 1–11

Contents lists available at ScienceDirect

Earth and Planetary Science Letters

journal homepage: www.elsevier.com/locate/epsl

Theoretical prediction for several important equilibrium Ge isotope fractionation factors and geological implications

Xuefang Li, Hui Zhao, Mao Tang, Yun Liu *

State Key Laboratory of Ore Deposit Geochemistry, Institute of Geochemistry, Chinese Academy of Sciences, Guiyang 550002, China

ARTICLE INFO

Article history:
Received 6 January 2009
Received in revised form 19 July 2009
Accepted 24 July 2009
Available online 29 August 2009

Editor: T.M. Harrison

Keywords:
Ge isotope
equilibrium isotope fractionation
quantum chemistry
Urey model

ABSTRACT

This study estimates equilibrium fractionation factors in the Ge isotope system, including the dominant aqueous $Ge(OH)_4$ and $GeO(OH)_3^-$ species in seawater, Ge-bearing organic complexes (e.g. Ge-catechol, Ge-oxalic acid and Ge-citric acid), and Ge in quartz- (or opal-), albite-, K-feldspar-, olivine- and sphalerite-like structures. Estimations are based on Urey model (or Bigeleisen–Mayer equation) and high level quantum chemistry calculations.

All calculations are made at B3LYP/6-311 + G(d,p) theory level. Solvation effects are treated by explicit solvent model ("water-droplet" method), and mineral structures are simulated using cluster models, in which the clusters are cut from the X-ray structures of those minerals. In addition, a number of different conformers are used for aqueous complexes in order to reduce the possible errors coming from the differences of configurations in solution. The "salt effect" on $GeO(OH)_{3(aq)}^-$ species is also carefully evaluated. We estimate the accuracy of these fractionation calculations at about ±0.3‰.

Excitedly, very large isotope fractionations are found between many Ge isotope systems. The Ge-containing sulfides (e.g. sphalerite) can extremely enrich light Ge isotopes (more than 10‰) compared with 4-coordinated Ge–O compounds (e.g. $Ge(OH)_{4(aq)}$ or quartz). The fractionations between $Ge(OH)_{4(aq)}$ and 6-coordinated Ge-bearing organic complexes can be also up to 4‰ at 25 °C. These results give a good explanation for the experimental observations of Rouxel et al. (2006). It also suggests a great potential for broad application of Ge isotope method in various geological systems.

1. Introduction

Germanium is a trace element, averaging about 1 ppm in the Earth's crust and natural waters. It has distinctly lithophile, siderophile, chalcophile, and organoplile properties depending on its environment (Bernstein, 1985). Because of their nearly identical ionic radii and chemical properties, Ge is often termed as a pseudoisotope of Si, and widely exists in silicates by substituting for Si in an amount up to a few ppm (Goldschmidt, 1958; De Argollo and Schilling, 1978; Bernstein, 1985; Froelich et al., 1985a,b; etc.). The highest concentrations of Ge, however, are found in two non-silicate materials (i.e. sulfides and coals).

In oceans, the two major sources of Ge and Si carry different Ge/Si ratios (μmol/mol) more than an order of magnitude (rivers: ~0.54 and hydrothermal fluids: ~8–14) (Shemesh et al., 1989). It has been proposed that Ge/Si ratios recorded by siliceous fossils might reflect the relative importance of those two sources (Shemesh et al., 1989; Froelich et al., 1992). Ge/Si ratios recorded in diatoms through the last 400 kyr demonstrate a systematic change over glacial–interglacial cycles (0.54 and 0.7–0.78 for glacial and interglacial periods, respectively) (Bareille et al., 1998; Mortlock et al., 1991). The ratios, therefore, were also used as a tracer of continental weathering intensity (Murnane and Stallard, 1990). There are, however, still many questions unsolved for Ge global cycling. Although the sources and sinks of Si in oceans are balanced, the Ge buried in opal, which is considered as the dominant sink for Ge, can only account for half of the Ge input (King et al., 2000; Hammond, et al., 2000; McManus et al., 2003). Consequently, there should be large missing sinks, possibly anoxic sediments (e.g. Hammond, et al., 2000), ferromanganese oxyhydroxides (King et al., 2000) or euxinic environments (sulfides extremely enrich light Ge isotopes and will be discussed below), suggesting that Ge might be decoupled from Si.

It is anticipated that Ge isotopes might provide additional constraints for the study of global Ge cycling. Ge has five stable isotopes ^{70}Ge, ^{72}Ge, ^{73}Ge, ^{74}Ge and ^{76}Ge with relative abundances of 21.2%, 27.7%, 7.7%, 35.9% and 7.5%, respectively. Using double spike isotope dilution and a hydride generation MC-ICP-MS technique, Siebert et al. (2006) measured the Ge isotope composition of high temperature spring fluids in the Cascade Range of the U.S. Pacific Northwest. Meanwhile, Rouxel et al. (2006) measured the Ge isotope composition for a number of igneous rocks and marine sediments, using a continuous flow hydride generation system coupled to a MC-ICP-MS instrument. Their results showed that Ge isotope fractionation follows a mass-dependent behavior. As the variation of $^{74}Ge/^{70}Ge$ ratios ($\Delta^{74}Ge$) is very small (0.25‰) for various mantle-derived rocks, including

* Corresponding author. Tel.: +86 851 5890798; fax: +86 851 5891664.
E-mail address: liuyun@vip.gyig.ac.cn (Y. Liu).

0012-821X/$ – see front matter © 2009 Elsevier B.V. All rights reserved.
doi:10.1016/j.epsl.2009.07.027

tholeiitic glasses from mid-ocean ridges, continental and volcanic island basalts, peridotite and granite, the authors concluded that the Δ^{74}Ge of Bulk Silicate Earth (BSE) should be equal to that of the igneous rocks and around 1.3‰ with respect to the standard they used. In addition, they found that the modern biogenic opals have a high Δ^{74}Ge between 2.0‰ and 3.0‰. Luais (2007) studied the small isotope fractionation of Ge in iron meteorites and pointed out such information could be used to distinguish some nebular condensation processes. These studies suggested that Ge isotopes show distinctive fractionation during a number of geologic processes. However, the lack of equilibrium fractionation parameters has severely limited our ability to explore further geological implications.

To date, no experiments have ever been carried out to determine Ge equilibrium isotope fractionation factors. Such experiments are often time-consuming and difficult to make. Instead, quantum chemistry calculations based on Urey model or Bigeleisen–Mayer equation (Urey, 1947; Bigeleisen and Mayer, 1947) may provide a promising alternative. Helped by advancements in computer technology, those calculations now can be made routinely with considerable precision. In this study, we calculate the equilibrium isotope fractionation factors between a number of important Ge-bearing systems, including the dominant aqueous Ge species in seawater, tetrahedral Ge oxides in quartz-, albite-, K-feldspar-, olivine-like structures, Ge-sulfides in a sphalerite-like structure and Ge-bearing organic complexes (Ge-catechol, Ge-oxalic acid, and Ge-citric acid in organic-rich fluids), which represent the major forms of Ge existing in nature. Those results might give an explanation for the pioneering studies of Siebert et al. (2006), Rouxel et al. (2006, 2008) and Luais (2007).

2. Theory and methods

2.1. Urey model or Bigeleisen–Mayer equation

Urey model or Bigeleisen–Mayer equation (Urey, 1947; Bigeleisen and Mayer, 1947) is the foundation for determining equilibrium isotope exchange constant K in stable isotope geochemistry. For an isotope exchange reaction:

$$A + B^* \leftrightarrow A^* + B \tag{1}$$

where A and A* differ only in isotope composition and A* is the one with heavier isotopes, K can be calculated from the ratios of the reduced isotope partition function ratio (RPFR) of those two molecules

$$K = \frac{RPFR(A)}{RPFR(B)} \tag{2}$$

Usually, fractionation factor α is used instead of K, e.g. $\alpha = K^{1/n}$, where n is the number of exchanged atom in the formula. Here, n equals 1 for all the Ge species discussed in this study, so $\alpha = K$. Since α is a number close to 1 and $10^3\ln(1.00X)$ approximately equals to X, the fractionation between A and B can be approximated more simply as $\Delta_{A-B} \approx 10^3 \ln\alpha$, which sometimes is called per mil fractionation in the field of isotope geochemistry (Sharp, 2005).

RPFR can be expressed in term of the harmonic normal-mode frequencies, ν_i, before and after isotope substitution

$$RPFR(A) = \frac{\sigma}{\sigma^*} \prod_i^{3n-6} \frac{u_i(A^*)\exp[-u_i(A^*)/2]\{1-\exp[-u_i(A)]\}}{u_i(A)\exp[-u_i(A)/2]\{1-\exp[-u_i(A^*)]\}} \tag{3}$$

where σ is symmetry number of the molecule and identical to σ^* for all Ge species here, and

$$u_i = \frac{h\nu_i}{kT}. \tag{4}$$

where, h and k are Plank and Boltzmann constants, respectively, and T is temperature in Kelvin. So, if we know all of the harmonic frequencies of one molecule with different isotopes, we can get the RFFR for that molecule. If we obtain the RPFRs for two molecules, we can determine the fractionation factor between those two molecules.

2.2. Methods of calculation

Early calculations of isotope fractionation were mainly based on experimentally measured spectroscopic data (Urey, 1947; Bigeleisen and Mayer, 1947; Richet, et al., 1977; Kieffer, 1982). Such calculations successfully predicted the directions, magnitudes, and temperature sensitivities of isotope fractionations for some simple gaseous phases, but could be limited by incompleteness and imprecision of spectroscopic data and occasional incorrect assignments of the vibrational data to a particular mode for complex systems and solids. Instead, *ab initio* quantum chemistry method has become a popular choice to compute directly harmonic vibrational frequencies (Hehre et al., 1986). The method has been widely used to calculate fractionation factors between some terrestrial samples (Criss, 1999; Driesner and Seward, 2000; Oi, 2000; Oi and Yanase, 2001; Schauble e al., 2003; Schauble, 2004; Jarzecki et al., 2004; Liu and Tossell, 2005; Zeebe, 2005; Tossell, 2005; Anbar et al., 2005; Schauble et al., 2006; Schauble, 2007; Seo et al. 2007; Rustad and Bylaska, 2007; Otake et al., 2008; Rustad et al., 2008; Rustad and Zarzycki, 2008). For example, Liu and Tossell (2005) successfully predicted the isotope fractionation factor between $B(OH)_3$ and $B(OH)_4^-$ in seawater, and their result was later confirmed by both experimental and computational studies (Klochko et al, 2006; Byrne et al, 2006; Rustad and Bylaska, 2007). In their study, solvation effect was simulated by the "water-droplet" (or super-molecule) model, in which the species of interest are surrounded by a large number of water molecules. Rustad et al. (2008) also presented a comprehensive review on quantum chemistry calculations of carbon isotope fractionations between CO_2(g), large aqueous supermolecular carbonate species, and carbonate minerals, using large molecular clusters, which is similar to the one used by Liu and Tossell (2005). They concluded that super-molecule-model-based quantum chemistry calculation is a promising method to seamlessly integrate the isotope fractionation calculations on gas, liquid and solid phases.

In our study, the B3LYP/6-311 + G(d,p) level (Becke, 1993; Lee, et al., 1988) is chosen for harmonic frequency calculation as a compromise between accuracy and computation cost. GAUSSIAN03 software package is used for the entire study (Frisch et al., 2003). For the frequency calculated with the 6-311 + G(d,p) basis set, Andersson and Uvdal (2005) recommended a scaling factor of 0.9679, which includes corrections for both inadequacy of quantum chemistry theoretical level and the anharmonicity contribution. However, for a specific isotope system, the scaling factor could be different from the recommended one which usually obtained from simple gaseous molecules. For example, in the calculation of boron isotope fractionation, Liu and Tossell (2005) used a larger scaling factor of 0.92 at HF/6-31G* level instead of the one (0.89) recommended by Scott and Radom (1996), and found that such a scaling factor could give a reasonable estimate of isotope fractionation. We therefore carefully tested the frequency scaling factor used here for B3LYP/6-311 + G(d,p) level.

Table 1 shows RPFRs and α factors of $Ge(OH)_4 \cdot 6H_2O$ and $GeO(OH)_3^- \cdot 6H_2O$ at different theoretical levels or scaling treatments. Most of the Ge systems we studied are similar to these two Ge species. We use four different conformers of each species and test five different theoretical levels. Four different frequency scaling treatments (i.e. 0.97, 1.00, 1.04 and 1.05) are also applied on the results of B3LYP/6-311 + G(d,p) level. As you can see, 1% change of the scaling factor will bring about 0.01‰ difference to the final fractionation numbers. The theoretical levels of B3LYP/aug-cc-pVTZ and B3LYP/6-311 + G(2df,p) are usually considered as the most precise ones for harmonic frequencies. They are also the most time-consuming ones among all the levels we tested (Note: the Supplementary data contains most of geometries and frequencies used in this paper). Their fractionation results are very similar (1.00078 vs. 1.00079), suggesting there is a converging point close to these two results

Table 1
RPFR and α results calculated in terms of $^{74}Ge/^{70}Ge$ for $Ge(OH)_4 \cdot 6H_2O$ and $GeO(OH)_3^- \cdot 6H_2O$ using 4 different conformers at B3LYP levels with different basis sets and frequency scaling factors (25 °C).

Clusters	RPFR							
	Basis set (scaling factor)							
	6-311G* (0.98)	6-311 + G(d,p) (0.97)	6-311 + G(d,p)	6-311 + G(d,p) (1.04)	6-311 + G(d,p) (1.05)	aug-cc-PVDZ	6-311 + G(2df,p)	aug-cc-pVTZ
$Ge(OH)_4$–$(H_2O)_6$_A	1.020058	1.019139	1.020193	1.021627	1.021990	1.020128	1.020920	1.020832
$Ge(OH)_4$–$(H_2O)_6$_B	1.019931	1.019054	1.020102	1.021528	1.021889	1.020064	1.020837	1.020753
$Ge(OH)_4$–$(H_2O)_6$_C	1.020054	1.019262	1.020321	1.021760	1.022125	1.020263	1.021054	1.020951
$Ge(OH)_4$–$(H_2O)_6$_D	1.019923	1.019240	1.020298	1.021736	1.022101	1.020226	1.021034	1.020919
Average	1.01999	1.01917	1.020229	1.021663	1.022026	1.02017	1.02096	1.02086
$GeO(OH)_3^-$–$(H_2O)_6$_A	1.018803	1.018199	1.019205	1.020574	1.020921	1.019149	1.019840	1.019796
$GeO(OH)_3^-$–$(H_2O)_6$_B	1.019454	1.018493	1.019514	1.020903	1.021255	1.019523	1.020208	1.020012
$GeO(OH)_3^-$–$(H_2O)_6$_C	1.019334	1.018752	1.019789	1.021199	1.021557	1.019794	1.020439	1.020403
$GeO(OH)_3^-$–$(H_2O)_6$_D	1.018831	1.018469	1.019489	1.020877	1.021229	1.019420	1.020123	1.020071
Average	1.01911	1.01848	1.019499	1.020888	1.021241	1.01947	1.02015	1.02007
$\alpha_{Ge(OH)_4\text{–}GeO(OH)_3^-}$	1.00086	1.00068	1.00071	1.00076	1.00077	1.00068	1.00079	1.00078

for B3LYP levels. The B3LYP/6-311 + G(d,p) level needs a large scaling factor (1.05) to let its result roughly match those of the two highest ones. This finding coincides with another test we performed on the Raman frequencies of aqueous $GeO_2(OH)_2^{2-}$ species. There are 18 water molecules surrounding $GeO_2(OH)_2^{2-}$ in the cluster model we used to calculate Raman spectra (Fig. 1). The calculated Raman frequencies at B3LYP/6-311 + G(d,p) and B3LYP/aug-cc-pVDZ levels and the experimental result are shown in Table 2. The experimental result is about 765 cm^{-1}, which is assigned mainly due to a symmetrical stretching of Ge O bonds in alkaline solution (Walrafen, 1964). The calculated frequencies of the symmetrical stretching modes are 736 cm^{-1} and 752 cm^{-1} for B3LYP/6-311 + G(d,p) and B3LYP//aug-cc-pVDZ levels. Obviously, B3LYP/6-311 + G(d,p) level underestimates vibrational frequencies for Ge compounds (Tables 1 and 2). Some studies (Akesson, et al., 1993, 1994; Rudolph and Pye, 1999; Rudolph, et al., 2000) pointed out that such vibrational frequency calculation problems are common for *ab initio* calculations and especially for heavy elements in solution with extra charges. Based on these results, we use a scaling factor (1.05) for B3LYP/6-311 + G(d,p) frequencies in this study.

2.3. "Water-droplet" method

In this study, solvation effects are simulated by the "water-droplet" method, in which the Ge species of interest are surrounded by a large number of water molecules. We initially add just a few (e.g. 6) water molecules surround each Ge species, then optimize the geometry and calculate frequencies. Subsequently, we add another 6 water molecules and do the optimization and frequency calculation again. Repeat this procedure until we finally get the intended number of water molecules. Importantly, we optimize every water-droplet cluster at B3LYP/6-311 + G** level all the time. From our experience, it is dangerous to pre-optimize the geometry at a lower level first, then re-optimize it at a higher level in an attempt to save time. It is dangerous because many systems we studied are loosely coordinated and a low theoretical level may produce incorrect local configuration. A wrong configuration produced at such circumstance usually may not be corrected by high level reoptimization for a large system.

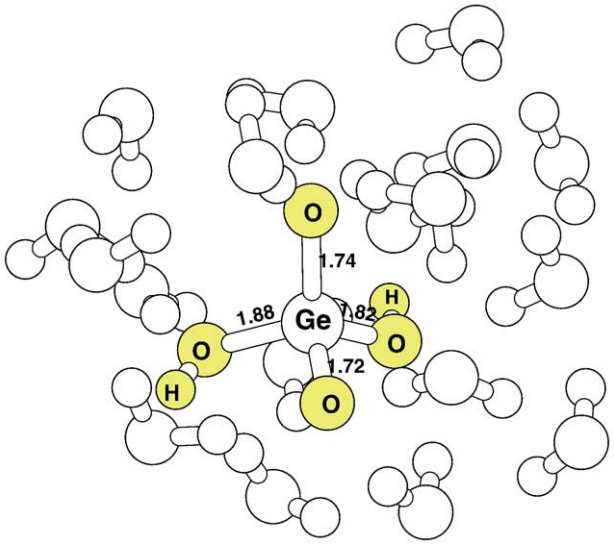

Fig. 1. Water-droplet cluster model for $GeO_2(OH)_2^{2-}$–$(H_2O)_{18}$ optimized at the B3LYP/6-311 + G(d,p) level. Bond lengths are in Angstrom (Å) for all models in this paper.

There are many different possible configurations for the Ge species in solution. One question is how to sample all important configurations. We don't have a perfect method to sample "all" important configurations. Instead, we have a quite simple way to sample several most important configurations. When we build the water-droplet models at each time, we just make sure the smallest water-droplets (i.e. the ones with 6 water molecules) are all different. This point can be easily checked after the optimization processes because the cluster models are very small. These smallest water-droplets also can be optimized to meaningful minimum energy points by modern quantum chemistry optimization algorithm (but cannot do so for large cluster models). Although we cannot guarantee they are at global minimum points, they should belong to a group with the lowest energies because it is not difficult to do that for a small system. Therefore, we actually have sampled several most important (or most popular) configurations for the smallest water-droplet. One exciting thing is that the first-coordination-shell configurations will not be significantly changed when more water molecules are added into the systems. It means these first-coordination-shell configurations are also important for larger water-droplet systems. However, the bond lengths and bond angles of the first-coordination-shell configurations can be slightly adjusted upon further addition of water molecules. Such adjustment indeed is important to accurately estimate solvation effect from outer shells of solvent molecules. We find that the variance of RPFR values of such

Table 2
Comparison of calculated and measured $GeO_2(OH)_2^{2-}$ Raman frequencies.

Calculated Raman frequencies (cm^{-1})			Experimental result (cm^{-1})
B3LYP/6-311 + G (d,p)	B3LYP/6-311 + G(d,p) (1.05)	B3LYP/aug-cc-pVDZ	
736	773	752	765

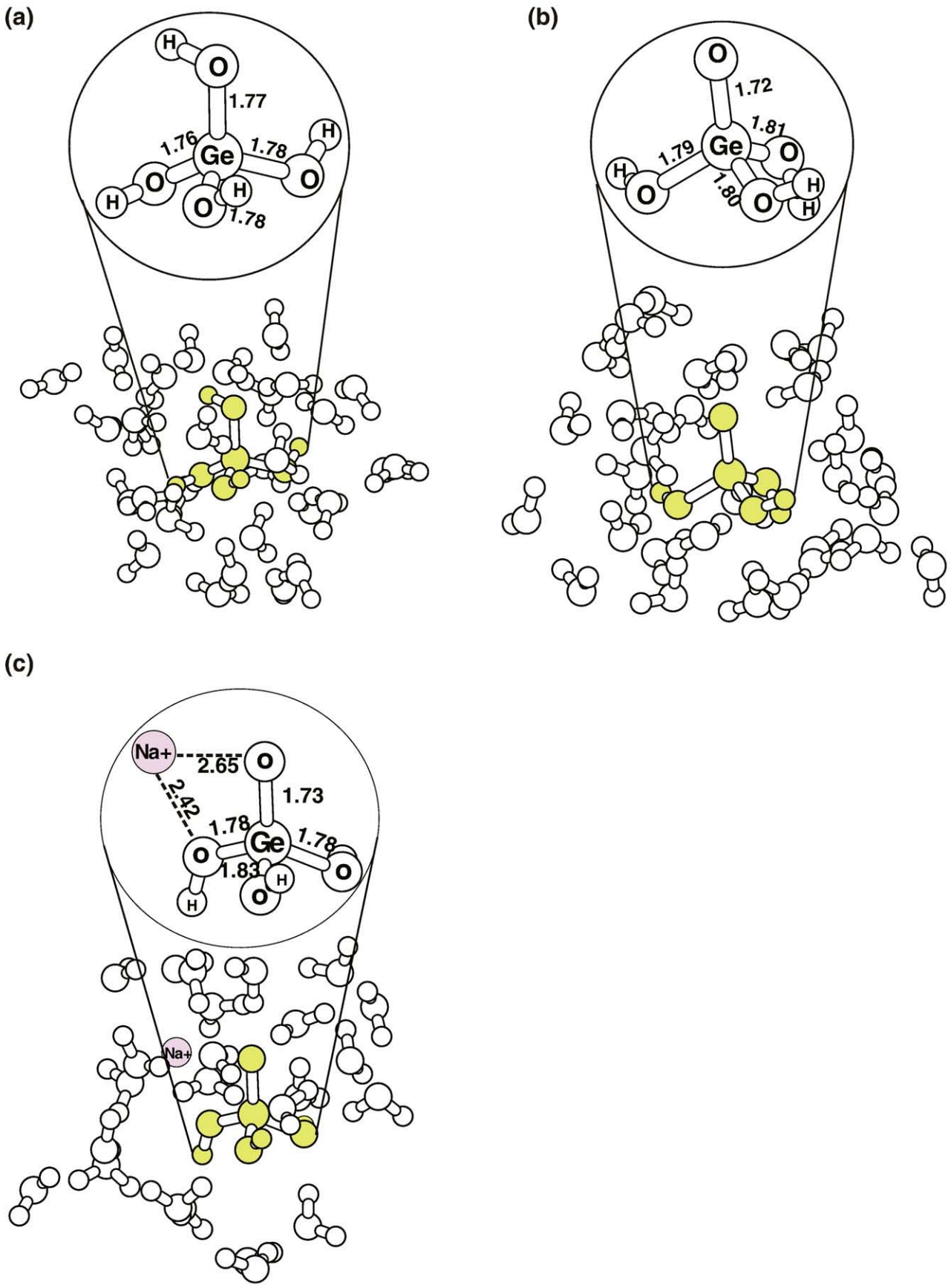

Fig. 2. Water-droplet cluster models for a) $Ge(OH)_4$–$(H_2O)_{30}$_A, b) $GeO(OH)_3^-$–$(H_2O)_{30}$_A and c) $GeO(OH)_3^-$–Na^+—$(H_2O)_{24}$. Magnified parts show the optimized central unit of each model.

important configurations usually is quite limited. Therefore, several sampling might narrow down the RPFR to a reasonable value. Usually, we use 12 sampling results to produce one final RPFR value.

3. Results

3.1. Fractionation between $Ge(OH)_4$ and $GeO(OH)_3^-$ in waters

In most natural waters (including seawater), Ge(IV) is coordinated with four oxygen atoms (Froelich et al., 1985a,b; Mortlock and Froelich, 1987), including the forms of $Ge(OH)_4$ and $GeO(OH)_3^-$ (Pokrovski and Schott, 1998a,b; Pokrovski et al., 2000). The fractionation between $Ge(OH)_4$ and $GeO(OH)_3^-$ thus is the basis for studying Ge isotope distribution in natural waters.

Geometry optimization and frequency calculations are carried out for all the water-droplet clusters of $Ge(OH)_4$ and $GeO(OH)_3^-$. Furthermore, four different water-droplets built from different starting structures (denoted respectively by A, B, C, D) are used to sample the important configurations. We get a series of water-droplets with 6, 12, 18, 24 and 30 water molecules, respectively. The examples of such water-droplets are shown in Fig. 2a and b for $Ge(OH)_4$ and $GeO(OH)_3^-$, where they are surrounded by 30 water molecules, respectively.

The four different configurations have slightly different RPFRs even when they have the same number of water molecules (Table 3). RPFRs are then plotted against the number of water molecules (6, 12, 18, 24 and 30, respectively) in Fig. 3. As a result, we choose the preferred RPFR is from the averages of the water-droplets with 18, 24 and 30 water molecules. In another words, the final RPFR is an average of 12 different conformers. The standard deviations, σ, from the 12 conformers are around 0.07‰ and 0.2‰ for $Ge(OH)_4$ and $GeO(OH)_3^-$, respectively. We also made some calculations at B3LYP/6-311G* level with up to 36 water molecules for $Ge(OH)_4$ and $GeO(OH)_3^-$ to check whether the RPFR is converged or not. The fractionations between $Ge(OH)_4$ and $GeO(OH)_3^-$ are 0.4‰ and 0.6‰ when calculated at the B3LYP/6-311G* and B3LYP/6-311 + G(d,p) levels, respectively (Table 3). Based on the results of Tables 1 and 3, we conclude that the accuracy of our calculations for fractionation factors should be better than ±0.3‰.

The water-droplet method can also be used to simulate the effect of salinity (the strength of ions) in seawater (Liu and Tossell, 2005). The cations in seawater mainly include Na^+, Li^+, Mg^{2+} and Ca^{2+}, etc. If $Ge(OH)_4$ and $GeO(OH)_3^-$ don't bond directly to them (i.e., outer-sphere interaction), the RPFRs won't be too much different from those in pure water. The positively charged cations mainly affect the negative ion $GeO(OH)_3^-$ due to electric attractions, but not the neutrally charged $Ge(OH)_4$. Here, we check the $GeO(OH)_3^-$–Na^+ species, as Na^+ accounts for 90% or more of all the cations in seawater. The calculations are similar to those for $Ge(OH)_4$ and $GeO(OH)_3^-$, and one of the $GeO(OH)_3^-$–Na^+–$(H_2O)_{24}$ super-molecules is showed in Fig. 2c. The RPFR of $GeO(OH)_3^-$–Na^+ in seawater is slightly larger than the one in pure water (Table 3), and the fractionation between $Ge(OH)_4$ and $GeO(OH)_3^-$ in seawater is about 0.3‰ lower than that in pure water.

PCM solution (Polarizable Continuum Models) built into the GAUSSIAN03 program (IEF-PCM) (Cances et al., 1997) is used for comparison. The PCM method is one of the most successful Self-Consistent Reaction Field (SCRF) methods (Tomasi, 1994) to simulate

Table 3
Results (in terms of $^{74}Ge/^{70}Ge$) calculated for $Ge(OH)_4$, $GeO(OH)_3^-$ and $GeO(OH)_3^-$–Na^+ using the water-droplet method (25 °C).

Cluster	RPFR [a]	RPFR [b]	Cluster	RPFR [a]	RPFR [b]	Cluster	RPFR [a]
$Ge(OH)_4$–$(H_2O)_6$_A	1.02199	1.020058	$GeO(OH)_3^-$–$(H_2O)_6$_A	1.020921	1.018803	$GeO(OH)_3^-$–Na^+–$(H_2O)_6$_A	1.021769
$Ge(OH)_4$–$(H_2O)_6$_B	1.021889	1.019931	$GeO(OH)_3^-$–$(H_2O)_6$_B	1.021255	1.019454	$GeO(OH)_3^-$–Na^+–$(H_2O)_6$_B	1.021889
$Ge(OH)_4$–$(H_2O)_6$_C	1.022125	1.020054	$GeO(OH)_3^-$–$(H_2O)_6$_C	1.021557	1.019334	$GeO(OH)_3^-$–Na^+–$(H_2O)_6$_C	1.021706
$Ge(OH)_4$–$(H_2O)_6$_D	1.022101	1.019923	$GeO(OH)_3^-$–$(H_2O)_6$_D	1.021229	1.018831	$GeO(OH)_3^-$–Na^+–$(H_2O)_6$_D	1.021672
Average	1.022026	1.01999	Average	1.021241	1.01911	Average	1.021759
$Ge(OH)_4$–$(H_2O)_{12}$_A	1.022136	1.020320	$GeO(OH)_3^-$–$(H_2O)_{12}$_A	1.021125	1.019126	$GeO(OH)_3^-$–Na^+–$(H_2O)_{12}$_A	1.021961
$Ge(OH)_4$–$(H_2O)_{12}$_B	1.022019	1.019891	$GeO(OH)_3^-$–$(H_2O)_{12}$_B	1.020796	1.018952	$GeO(OH)_3^-$–Na^+–$(H_2O)_{12}$_B	1.021887
$Ge(OH)_4$–$(H_2O)_{12}$_C	1.021919	1.019880	$GeO(OH)_3^-$–$(H_2O)_{12}$_C	1.021626	1.019686	$GeO(OH)_3^-$–Na^+–$(H_2O)_{12}$_C	1.021742
$Ge(OH)_4$–$(H_2O)_{12}$_D	1.022096	1.020188	$GeO(OH)_3^-$–$(H_2O)_{12}$_D	1.021211	1.019132	$GeO(OH)_3^-$–Na^+–$(H_2O)_{12}$_D	1.021548
Average	1.022043	1.02007	Average	1.021190	1.01922	Average	1.021785
$Ge(OH)_4$–$(H_2O)_{18}$_A	1.022167	1.020113	$GeO(OH)_3^-$–$(H_2O)_{18}$_A	1.021140	1.019052	$GeO(OH)_3^-$–Na^+–$(H_2O)_{18}$_A	1.021887
$Ge(OH)_4$–$(H_2O)_{18}$_B	1.022096	1.020092	$GeO(OH)_3^-$–$(H_2O)_{18}$_B	1.021342	1.019293	$GeO(OH)_3^-$–Na^+–$(H_2O)_{18}$_B	1.021657
$Ge(OH)_4$–$(H_2O)_{18}$_C	1.022031	1.020063	$GeO(OH)_3^-$–$(H_2O)_{18}$_C	1.021233	1.019297	$GeO(OH)_3^-$–Na^+–$(H_2O)_{18}$_C	1.021684
$Ge(OH)_4$–$(H_2O)_{18}$_D	1.022173	1.020175	$GeO(OH)_3^-$–$(H_2O)_{18}$_D	1.021350	1.019394	$GeO(OH)_3^-$–Na^+–$(H_2O)_{18}$_D	1.021883
Average	1.022117	1.02011	Average	1.021266	1.01926	Average	1.021778
$Ge(OH)_4$–$(H_2O)_{24}$_A	1.022191	1.020113	$GeO(OH)_3^-$–$(H_2O)_{24}$_A	1.021449	1.019529	$GeO(OH)_3^-$–Na^+–$(H_2O)_{24}$_A	1.021779
$Ge(OH)_4$–$(H_2O)_{24}$_B	1.022122	1.019854	$GeO(OH)_3^-$–$(H_2O)_{24}$_B	1.021489	1.019447	$GeO(OH)_3^-$–Na^+–$(H_2O)_{24}$_B	1.021610
$Ge(OH)_4$–$(H_2O)_{24}$_C	1.022247	1.020126	$GeO(OH)_3^-$–$(H_2O)_{24}$_C	1.021331	1.019367	$GeO(OH)_3^-$–Na^+–$(H_2O)_{24}$_C	1.021792
$Ge(OH)_4$–$(H_2O)_{24}$_D	1.022216	1.020176	$GeO(OH)_3^-$–$(H_2O)_{24}$_D	1.021720	1.019994	$GeO(OH)_3^-$–Na^+–$(H_2O)_{24}$_D	1.021678
Average	1.022194	1.02007	Average	1.021497	1.01958	Average	1.021778
$Ge(OH)_4$–$(H_2O)_{30}$_A	1.022204	1.020263	$GeO(OH)_3^-$–$(H_2O)_{30}$_A	1.021525	1.019672	**Preferred value**	**1.02176**
$Ge(OH)_4$–$(H_2O)_{30}$_B	1.022167	1.018628	$GeO(OH)_3^-$–$(H_2O)_{30}$_B	1.021559	1.019587	σ	1.2e−04
$Ge(OH)_4$–$(H_2O)_{30}$_C	1.022030	1.020145	$GeO(OH)_3^-$–$(H_2O)_{30}$_C	1.021794	1.019766		
$Ge(OH)_4$–$(H_2O)_{30}$_D	1.022016	1.020028	$GeO(OH)_3^-$–$(H_2O)_{30}$_D	1.021973	1.020089		
Average	1.022104	1.01977	Average	1.021713	1.01978		
Preferred value	**1.02214**	**1.01998**	**Preferred value**	**1.02149**			
σ	7.5e−05		σ	2.3e−04			
			$GeO(OH)_3^-$–$(H_2O)_{36}$_A		1.019489		
			$GeO(OH)_3^-$–$(H_2O)_{36}$_B		1.019841		
			$GeO(OH)_3^-$–$(H_2O)_{36}$_C		1.019841		
			$GeO(OH)_3^-$–$(H_2O)_{36}$_D		1.018070		
			Average		1.01931		
			Preferred value		**1.01959**		
A–B	Δ [a] $_{A-B}$(‰)		Δ [b] $_{A-B}$(‰)	A–B			Δ [a] $_{A-B}$(‰)
$Ge(OH)_4$–$GeO(OH)_3^-$	0.6		0.4	$Ge(OH)_4$–$GeO(OH)_3^-$–Na^+			0.4

The bold values are preferred ones.
[a] Data were calculated at B3LYP/6-311 + G(d,p) level, with frequency scaling factor 1.05.
[b] Data were calculated at B3LYP/6-311G* level, with 0.98 frequency scaling factor.

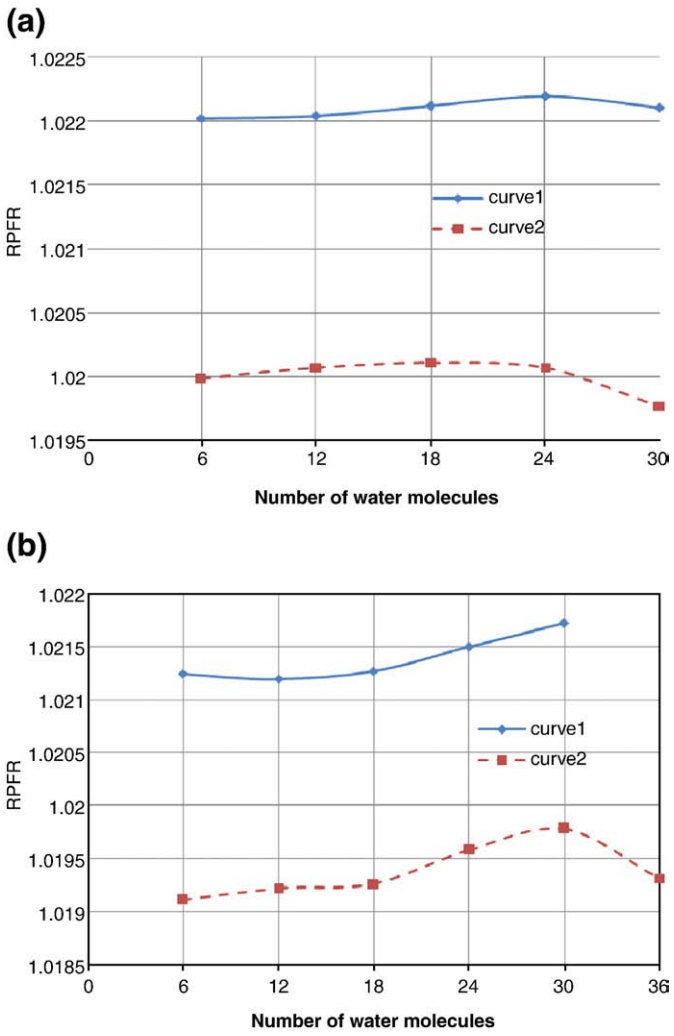

Fig. 3. RPFR vs. the number of water molecules for a) $Ge(OH)_4$ and b) $GeO(OH)_3^-$ in water-droplet cluster models. Curves 1 and 2 denote models computed at the B3LYP/6-311+G(d,p) level (with 1.05 frequency scaling factor), and at B3LYP/6-311G* level (with 0.98 frequency scaling factor), respectively.

solvent effects, and has been used to calculate the iron isotope fractionation between $Fe(H_2O)_6^{3+}$ and $Fe(H_2O)_6^{2+}$ (Jarzecki et al., 2004; Anbar et al., 2005). It places the solute in a cavity within solvent reaction field. The cavity is a series of overlapping spheres containing the solute molecule and solvent outside of the cavity is modeled as a continuum of uniform dielectric constant. The PCM method, however, does not give a proper treatment of strong hydrogen bonding in solution, in particular for those species with high negative charges (personal communication with author of Gaussian). In addition, the PCM sometimes assumes the highest symmetry with identical bond lengths for all Ge–O (Fig. 4), and it cannot be changed even we have added a "nosymm" (not assume any symmetry) keyword in the input file. However, it is not realistic as the hydrogen bond formed with the outer-layer of the water molecules can't be the same at different directions. Here, we find that there are noticeable differences between the RPFRs calculated with PCM vs. explicit solution especially for the $GeO(OH)_3^-$, despite similar bond lengths (Table 4). Based on the discussion above, it is therefore better to consider the solvation effect using the more time-consuming but safer "water-droplet" method.

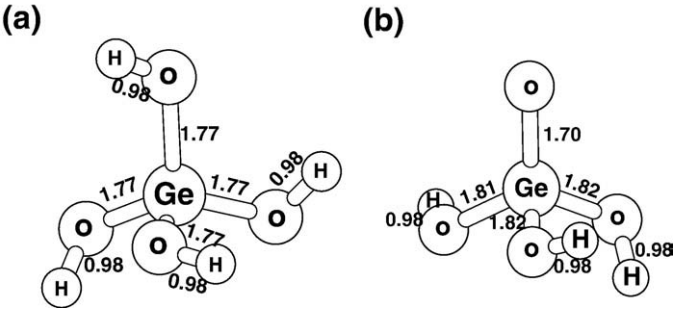

Fig. 4. Structure models for a) $Ge(OH)_4$ and b) $GeO(OH)_3^-$ using PCM method.

Table 4
Comparison of bond lengths, RPFRs and fractionation factors calculated using the water-droplet (putting 30 water molecules) and PCM methods (25 °C).

	Water-droplet		PCM	
	Ge–O (Å)	RPFR	Ge–O (Å)	RPFR
$Ge(OH)_4$	1.76–1.78	1.02214	1.77	1.020045
$GeO(OH)_3^-$	1.72–1.81	1.02149	1.70–1.82	1.018821
$\Delta_{Ge(OH)_4-GeO(OH)_3^-}$ (‰)	0.6		1.2	

3.2. The fractionations from Ge-bearing organic complexes

Unlike Si, Ge can form chelate complexes with organic matter (Bernstein, 1985). Pokrovski et al. (2000) presented a detailed study on the structures of Ge-organic ligand complexes in aqueous solution, using an X-ray absorption fine structure spectroscopy. They found that Ge can enlarge its coordination from 4 to 6 to form chelate type complexes with di- and polyfunctional carboxylic acids, polyalcohols and ortho-diphenols.

Here, we make some calculations on Ge-catechol, Ge-oxalic acid, Ge-citric acid complexes with phenolic and carboxylic functional groups. For these species, geometry optimization and frequency calculations are made with up to 18 water molecules (Fig. 5). Our results show the same coordination numbers (i.e. 6) as Pokrovski et al. (2000), suggesting that these complexes indeed are stable in solution. We have also reproduced two structures of a Ge_citric acid chelated complex, which involves two carboxyls and two hydroxyls with formation of di-dentate and tri-dentate chelate complexes. The mean Ge–O bond lengths of the four species are around 1.92–2.00 Å, slightly larger than those of Pokrovski et al., which are from 1.85 to 1.94 Å. For the RPFRs, we choose the average values of water-droplet clusters with 6, 12 and 18 water molecules (Table 5). Standard deviations are less than 0.1‰ for all of the species. The organic complexes can be greatly fractionated, enriched in light Ge isotopes relative to coexisting aqueous $Ge(OH)_4$.

3.3. Fractionation in quartz-, albite-, K-feldspar- and olivine-like structures

In addition, we also calculate fractionations of Ge isotopes in some of the major rock-forming minerals in the earth's crust, including quartz, albite, K-feldspar and olivine. We built a number of clusters to represent those minerals. This method has already been used to study the "local" properties of silicate minerals (Gibbs, 1982; Lasaga and Gibbs, 1990). The isotopic effect is mainly a local property, and hence can be studied by cluster method. Usually, the isotopic effect will decay quickly from 2 or 3 bonds away. Cluster models thus may be adequate to calculate isotope fractionations in crystalline materials (Liu and Tossell, 2005).

To build a cluster model, a portion of structure is cut out from the X-ray structures of each mineral. Then we use common methods, such as adding H atoms, etc. to treat the dangling bonds. These expedients appear to have negligible effects on the central atom of interest. We always make sure that the total charge is close to zero. Similar strategies have been used to

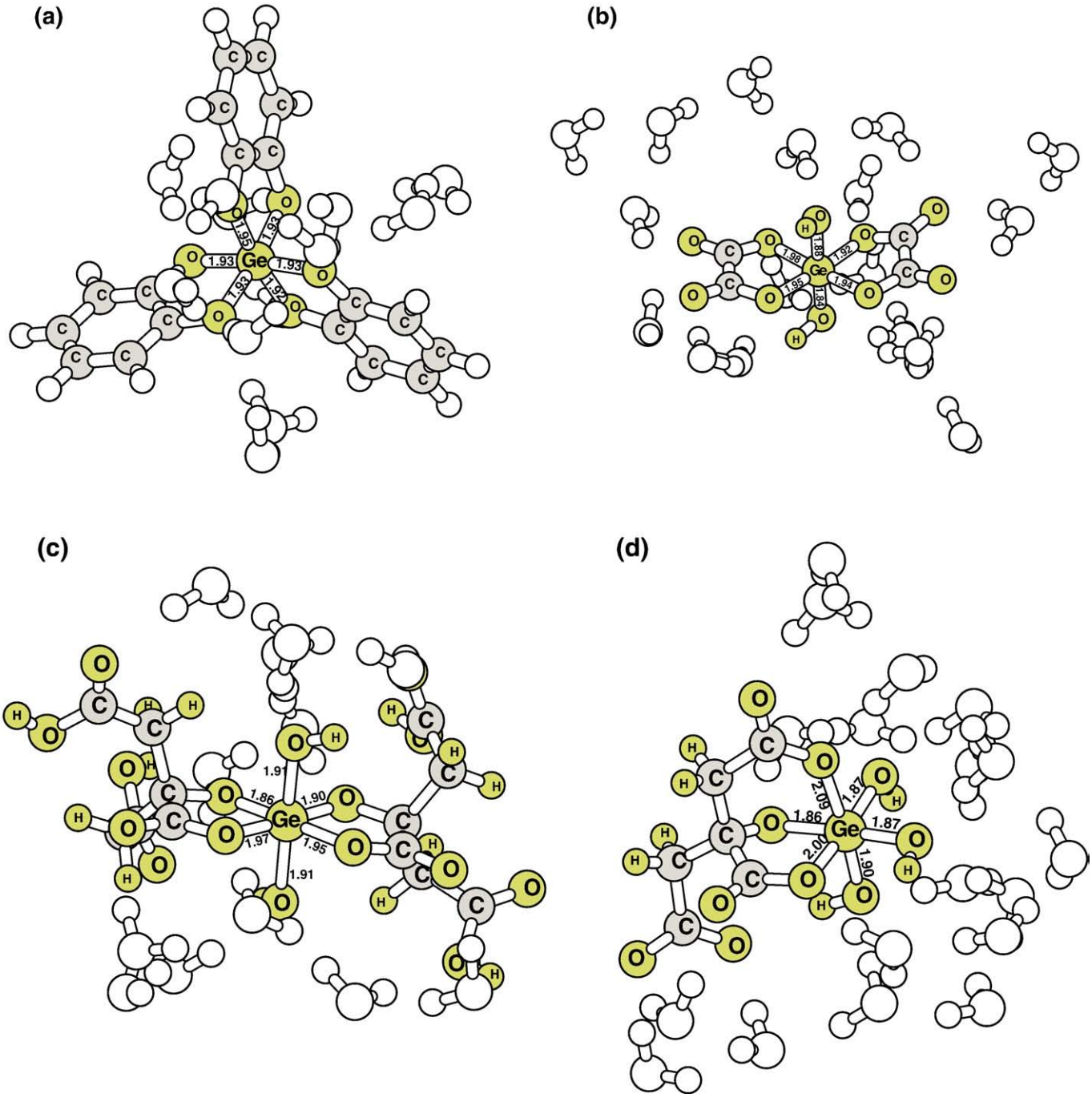

Fig. 5. Cluster models for a) Ge-catechol–$(H_2O)_{18}$, b) Ge-oxalic acid–$(H_2O)_{18}$, c) Ge-(citric acid)$_2$– $(H_2O)_{18}$ and d) Ge-citric acid–$(H_2O)_{18}$.

study the NMR properties for many minerals and silicate melts before (e.g. Liu et al., 2002; Liu and Nekvasil, 2002; Liu and Tossell, 2003). This "supermolecule" method has also been advocated recently to calculate the carbon isotope fractionation by Rustad et al. (2008) and Rustad and Zarzycki (2008). In their study, a modified version of Eq. (3) without μ_i (A*)/μ_i(A) ratio is used to calculate RPFRs of minerals because they think that there are no rotational and translational terms in a crystal, especially they used partial Hessian analysis treatments (e.g. Head, 1997) for obtaining interested vibrational frequencies from large cluster models. Here, we still use Eq. (3) to calculate RPFR of the minerals because the sizes of our cluster models are smaller and an explanation is given in the Supplementary data. Fig. 6 shows optimized structure of the clusters. The relationship between mean bond length of Ge–O and calculated RPFRs is shown in Table 6. There is a linear dependence between bond lengths and RPFRs (Fig. 7), suggesting that fractionations, to a certain extent, are determined by the Ge–O bond strength in these minerals. Fractionations between minerals and $Ge(OH)_{4(aq)}$ show a large variation, from 1.1‰ for quartz to −1.3‰ for olivine.

3.4. Temperature effect on Ge isotope fractionations

The theoretical fractionation curves with respect to $Ge(OH)_4$ are plotted against temperature for some Ge-bearing species and minerals (Fig. 8). There is little temperature effect on the fractionation between Ge $(OH)_4$ and $GeO(OH)_3^-$ in natural waters. In contrast, a significant decrease can be seen on the fractionations between Ge-bearing organic matter and

Table 5
Results computed for Ge-bearing organic complexes using the water-droplet method (25 °C).

Cluster	RPFR	Cluster	RPFR
Ge-catechol–$(H_2O)_6$	1.017031	Ge-oxalic acid–$(H_2O)_6$	1.018033
Ge-catechol–$(H_2O)_{12}$	1.017130	Ge-oxalic acid–$(H_2O)_{12}$	1.018409
Ge-catechol–$(H_2O)_{18}$	1.017203	Ge-oxalic acid–$(H_2O)_{18}$	1.018094
Preferred value	**1.01712**	**Preferred value**	**1.01818**
σ	7.0e−05	σ	1.6e−04
Ge-citric acid (a)–$(H_2O)_6$	1.018052	Ge-citric acid (b)–$(H_2O)_6$	1.017537
Ge-citric acid (a)–$(H_2O)_{12}$	1.017914	Ge-citric acid (b)–$(H_2O)_{12}$	1.017804
Ge-citric acid (a)–$(H_2O)_{18}$	1.017911	Ge-citric acid (b)–$(H_2O)_{18}$	1.017692
Preferred value	**1.01796**	**Preferred value**	**1.01768**
σ	6.6e−05	σ	1.1e−04
Δ_{A-B}(‰)			
$\Delta_{\text{Ge-catechol–Ge(OH)}_4}$	−4.9	$\Delta_{\text{Ge-oxalic acid–Ge(OH)}_4}$	−3.9
$\Delta_{\text{Ge-citric acid(a)–Ge(OH)}_4}$	−4.1	$\Delta_{\text{Ge-citric acid(b)–Ge(OH)}_4}$	−4.4

The bold values are preferred ones (see the text).

Table 6
Mean Ge–O or Ge–S bond lengths and RPFRs calculated for Ge in quartz, albite, K-feldspar, olivine, and sphalerite-like structures $[Ge^{II}S_4Zn_2]^{2-}$ and $[Ge^{IV}S_4Zn_4]^{2+}$. Fractionation relative to $Ge(OH)_4$ and the quartz-like structure (25 °C).

Minerals	Ge–O or Ge–S (Å)	RPFR	$\Delta_{\text{mineral–Ge(OH)4}}$ (‰)	$\Delta_{\text{mineral–quartz}}$ (‰)
Quartz	1.753	1.02325	1.1	0.0
Albite	1.760	1.02250	0.4	−0.7
K-feldspar	1.758	1.02277	0.6	−0.5
Olivine	1.790	1.02080	−1.3	−2.4
$[Ge^{II}S_4Zn_2]^{2-}$	2.257	1.00976	−12.2	−13.3
$[Ge^{II}S_4Zn_4]^{2+}$	2.267	1.01045	−11.5	−12.6
$[Ge^{IV}S_4Zn_2]^{0}$	2.275	1.01055	−11.4	−12.5

$Ge(OH)_4$, but even at 100 °C the fractionations are larger than 2‰. The temperature effect on quartz-solution fractionation is significant. The fractionation between that mineral and $Ge(OH)_4$ at 80 °C is roughly half of that at 25 °C. The fractionation is slightly larger than those for albite and K-feldspar. On the other hand, the fractionation between olivine and $Ge(OH)_4$ is around −1.3‰ at 25 °C and in the opposite direction to those calculated for the rest of the minerals. We have also provided a simple ($A*10^6/T^2 + B$)-type formula (see Table 7) to facilitate calculations of the temperature effect on the fractionations between quartz, albite, K-feldspar, olivine and $Ge(OH)_4$ or quartz.

3.5. Preliminary results on Ge-bearing sulfides

Germanium can be Ge(II) instead of Ge(IV) in some sulfides. Smaller valence states usually mean weaker bonding; second, even as Ge(IV), the

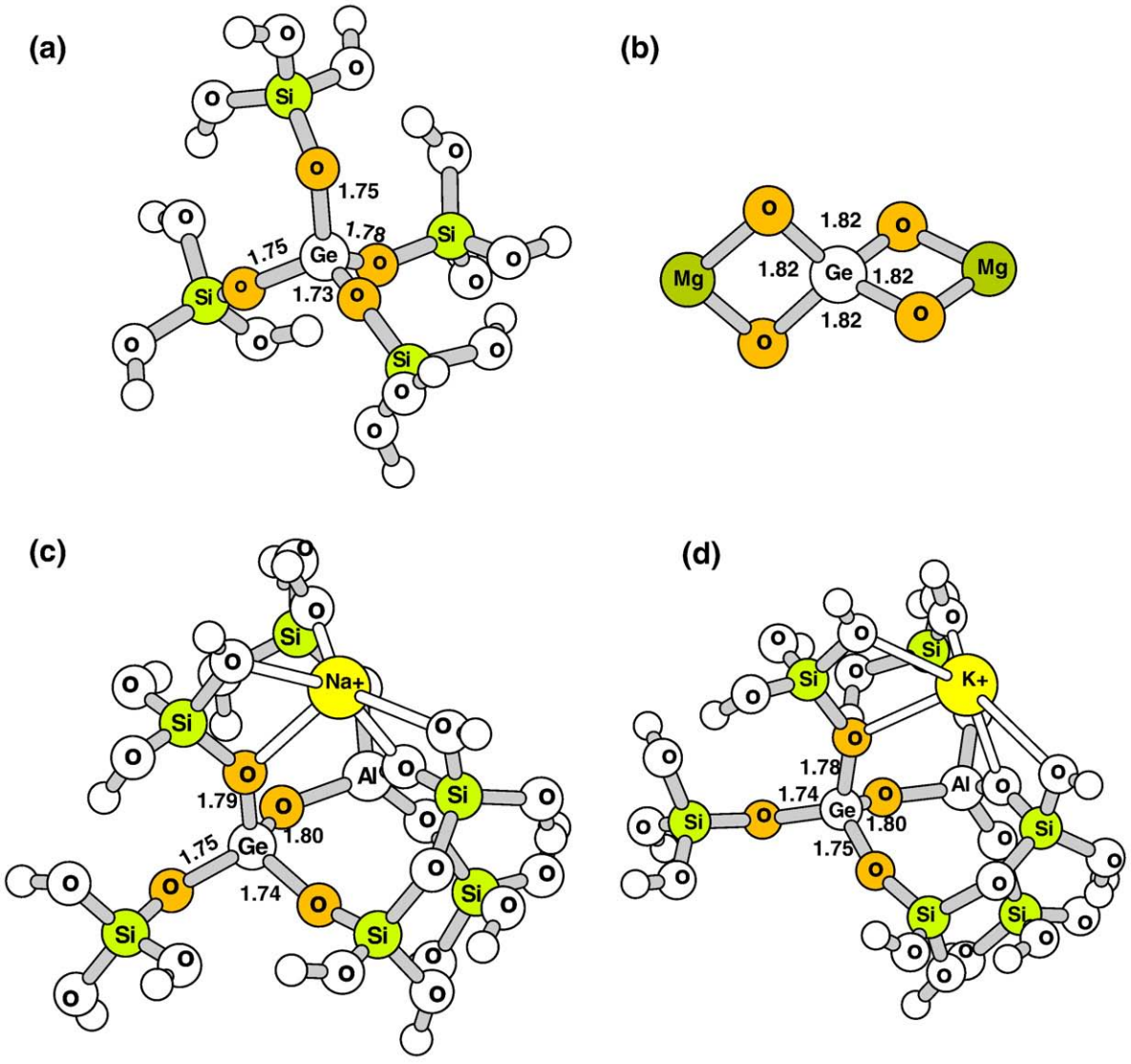

Fig. 6. Cluster models of a) quartz-, b)olivine-, c) albite- and d) K-feldspar-like structures.

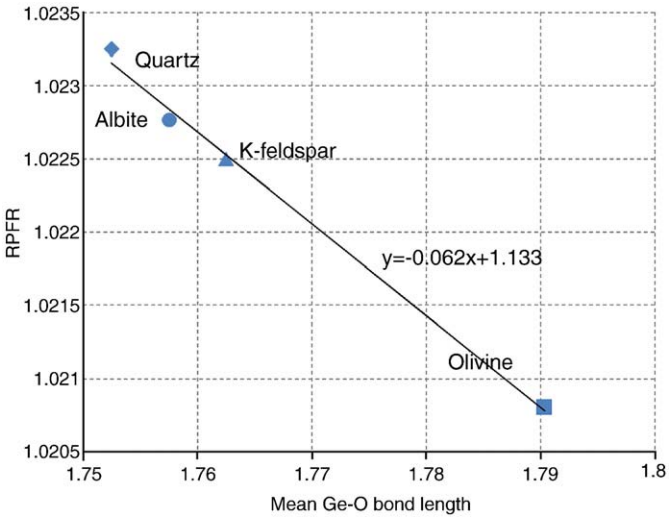

Fig. 7. Dependence of the mean Ge–O bond lengths and RPFRs in quartz, albite, K-feldspar and olivine-like structures.

Table 7
Formulae for calculating fractionation factors vs. *T*.

Δ (‰)	$A*10^6/T^2+B$
$\Delta_{Ge(OH)_4-Ge(OH)_3^-}$	$0.04*10^6/T^2+0.19$
$\Delta_{Ge\text{-}catechol-Ge(OH)_4}$	$-0.30*10^6/T^2-1.56$
$\Delta_{quartz-Ge(OH)_4}$	$0.12*10^6/T^2-0.23$
$\Delta_{albite-Ge(OH)_4}$	$0.06*10^6/T^2-0.34$
$\Delta_{(K\text{-}feldspar)-Ge(OH)_4}$	$0.08*10^6/T^2-0.29$
$\Delta_{olivine-Ge(OH)_4}$	$-0.08*10^6/T^2-0.43$
$\Delta_{quartz-albite}$	$0.05*10^6/T^2+0.11$
$\Delta_{quartz-(K\text{-}feldspar)}$	$0.04*10^6/T^2+0.06$
$\Delta_{quartz-olivine}$	$0.19*10^6/T^2+0.20$

Ge–S co-valent bond is much weaker than the Ge–O bond. Therefore, it is possible that sulfides have extremely low $^{74}Ge/^{70}Ge$.

We used three crude cluster models $[Ge(II)S_4Zn_2]^{2-}$, $[Ge(II)S_4Zn_4]^{2+}$ and $[Ge(IV)S_4Zn_2]^0$ to simulate sphalerite-like structures (Fig. 9). To prevent distortion of the $[GeS_4]$ tetrahedron, the dihedral angles of each tetrahedron were fixed to 120° and the four Ge–S bond lengths were constrained to be equal. The RPFR of $[Ge(II)S_4Zn_2]^{2-}$ is 1.00976 and that for $[Ge(II)S_4Zn_4]^{2+}$ is 1.01045 at 25 °C (Table 6). The fractionations

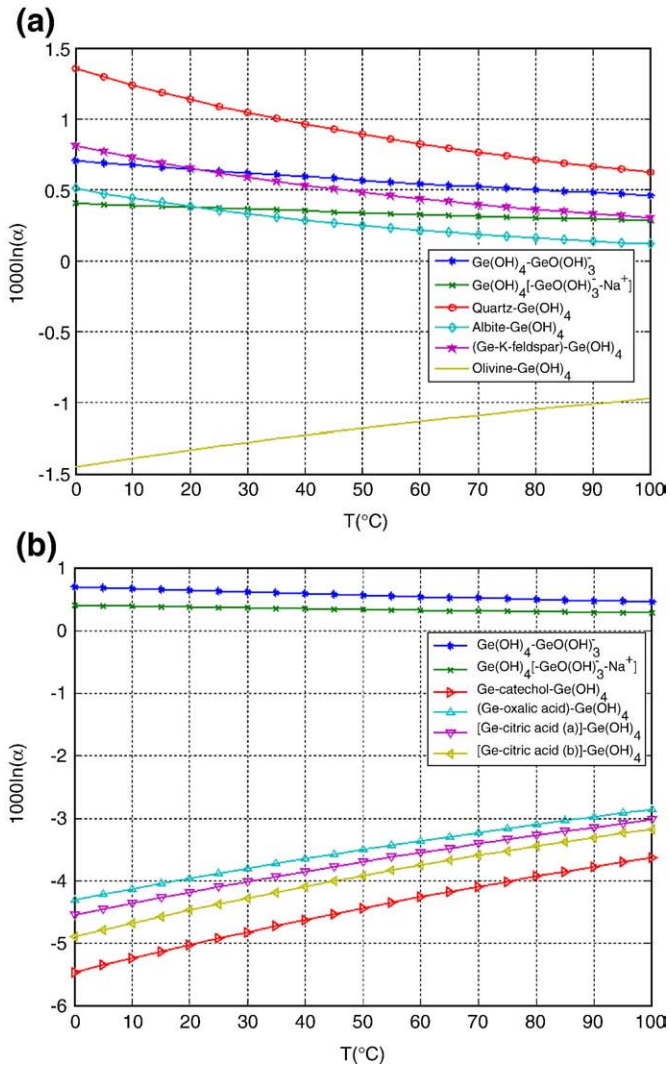

Fig. 8. The curves of theoretical fractionation (1000lnα) vs. *T* for important aqueous Ge species and rock-forming minerals. a) Minerals relative to aqueous $Ge(OH)_4$ and b) organic complexes relative to aqueous $Ge(OH)_4$. The $Ge(OH)_4$–$GeO(OH)_3^-$ and $Ge(OH)_4$–$GeO(OH)_3^-$–Na^+ fractionations are also plot as reference.

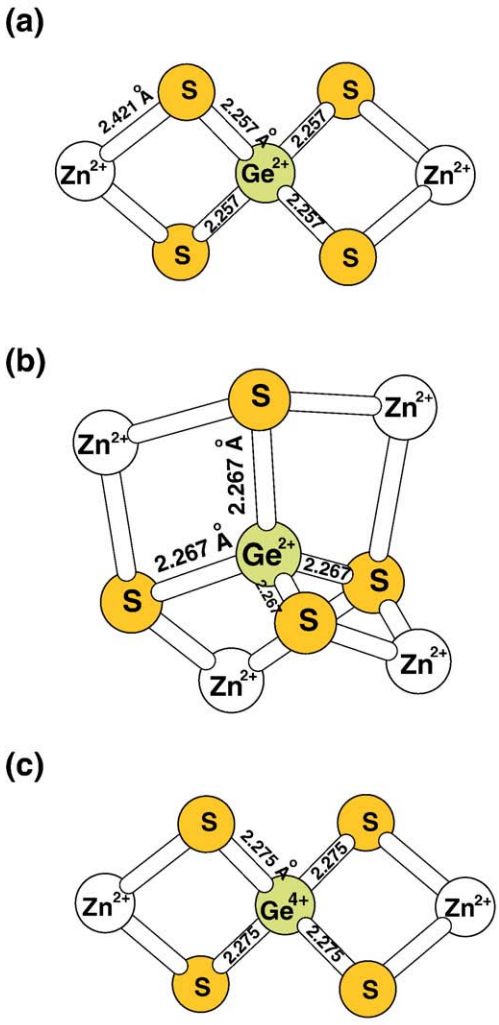

Fig. 9. Simple sphalerite-like cluster models for a) $[Ge(II)S_4Zn_2]^{2-}$, b) $[Ge(II)S_4Zn_4]^{2+}$ and c) $[Ge(IV)S_4Zn_2]^0$.

between these two simple sphalerite-like structures and the $Ge(OH)_{4(aq)}$ species are 12.2‰ and 11.5‰, respectively. The $[Ge(IV)S_4Zn_2]^0$ cluster (Fig. 9c) produces a RPFR of 1.01055 and $\Delta_{Ge(OH)4(aq)-[Ge(IV)S4Zn2]}$ only is only slightly changed to 11.4‰ compared with the results of Ge(II) clusters. Larger sphalerite cluster models coupled with partial Hessian analysis treatment (e.g. Head, 1997) are expected to produce better fractionation numbers. However, based on the preliminary results of these simple Ge-bearing sulfide models, we can easily conclude that Ge in sulfides could be extremely light relative to Ge-containing oxides or silicates.

4. Discussion

Fractionation between the dominant $Ge(OH)_4$ and $GeO(OH)_3^-$ species in pure water is small (about 0.6‰), and even smaller in seawater (around 0.4‰). The fractionation between the two species thus has little effect on Ge isotope distribution of natural waters. However, a large fractionation to light Ge isotopes could happen if organic matter is involved. Pokrovski and Schott (1998b) suggested that the complexation of Ge with aqueous humic and fulvic acids having carboxylic and phenolic functional groups could lead to a significant increase in Ge/Si ratios in the organic-rich rivers, and raised a caution on the use Ge/Si ratios in organic-rich rivers for estimating chemical weathering intensity on continent (Murnane and Stallard, 1990). Here, we predict that the organic-complexed Ge should be highly enriched in light Ge isotopes. Ge isotope composition therefore might be used as an index to distinguish possible bio-involvement in those environments, if we can also exclude the involvement of sulfides. Our calculations suggest that organic-rich and euxinic environments could form reservoirs of light Ge isotopes, including the super-large Lincang Ge ore-deposit hosted in a tertiary coal-bearing basin in Yunnan province, China (Hu et al., 1996), and in black shale series formed under anoxic or euxinic conditions.

Siebert et al. (2006) reported Ge isotope compositions of several high temperature hydrothermal fluids. The signs of Ge isotope composition numbers reported in their paper were reversed due to a well hidden but simple division error (private communication with Dr. Siebert). They actually observed the high Ge/Si ratio (up to 74 μmol/mol) and *heavy* Ge isotopes relative to Columbia River basalt in the high temperature hydrothermal fluids. It is very difficult to explain why hydrothermal fluids are enriched in Ge isotopes. Our calculations show that the quartz-like structure will enrich heavy Ge isotopes relative to $Ge(OH)_{4(aq)}$. Previous studies suggested that precipitation of quartz is the dominant control of the Ge/Si ratio for hydrothermal fluids (Holland and Malinin, 1979; Fournier, 1985; Evans and Derry, 2002). Therefore, Ge isotope compositions of the fluids would be controlled by fractionations between quartz and the dominant Ge species in solution, leading to an enrichment of light Ge isotopes in the fluid. This contradicts with the results of Siebert et al. (2006). There could be other unknown reasons to explain the high Ge/Si ratio and heavy Ge isotopic compositions of continental hydrothermal fluids. In the light of the equilibrium fractionation factors provided in this study, we hypothesize that the precipitation of Ge-bearing sulfides maybe one of the potential causes.

Our results may provide an explanation for the work of Rouxel et al. (2006). In their paper, they argued that the high Δ^{74}Ge observed in opal sponges should be a lower bound on Δ^{74}Ge of modern seawater, such that modern seawater could be highly enriched in heavy Ge isotopes. This agreement is based on the observation that marine sponges are preferably enriched in light Si isotopes (De La Rocha, 2003) and the expectation that the fractionation mechanisms of Ge and Si be similar to each other. This scenario is very possible if Ge, like Si, is transported into diatoms by organic transporters (e.g. Hildebrand et al., 1997; Hildebrand, 2000; Sumper and Brunner, 2008). As we have shown in this study, organic complexes tend to acquire lighter Ge isotope compositions compared to $Ge(OH)_{4(aq)}$. Such a high Δ^{74}Ge of seawater, however, would require fairly large reservoirs of light Ge isotopes. Where are these reservoirs or sinks? Galy et al. (2002) found that Ge absorption processes on the surfaces of Fe-oxyhydroxides could lead to an enrichment of heavy Ge isotopes in seawater up to 0.75‰ (^{74}Ge/^{72}Ge). This observation has been confirmed by Rouxel et al. (2008b). Therefore, Fe-oxyhydroxides could be one of the so-called Ge "missing sink" (e.g. King et al., 2000). Its effect on the global Ge isotope budget in seawater is still unclear, as there is no fractionation factor data for such adsorption processes. In addition, our calculations on fractionation of Ge isotopes in Ge-bearing sulfides suggest a huge fractionation (up to 10‰ at 25 °C) relative to aqueous $Ge(OH)_{4(aq)}$. Ge-bearing sulfides, therefore, may represent an even more important sink of light Ge isotopes.

The Ge isotope composition of modern seawater is crucial for establishing global Ge isotope fluxes. Studies are underway to determine the Ge isotope composition of seawater (i.e. Rouxel et al. 2008). Combined with the equilibrium fractionation factors provided here, we can begin to speculate the global cycling of Ge isotopes.

Finally, our calculations show that fractionations of Ge in albite and K-feldspar relative to quartz are small, suggesting that their Ge isotope compositions can be treated as the same in rocks during high temperature equilibrium process. This agrees well with existing evidence that all the igneous rocks have very similar Ge isotope compositions (Rouxel et al., 2006). As Ge in olivine-like structure prefers lighter isotopes compared to $Ge(OH)_4$, with a fractionation about −1.3‰, there might be an additional contribution to the heavy Ge isotope composition of seawater if there was an equilibrium isotope exchange process between the sea-floor basalt and seawater.

5. Conclusions

In this study, we estimate the equilibrium isotope fractionation factors between several important Ge isotope systems. Our results show that there should be distinct fractionations of Ge isotopes in a number of different geological processes. We predict that Ge-bearing sulfides will be highly enriched in light Ge isotopes relative to Ge oxides. In addition, we suggest that Ge isotopes may be used as an indicator for biological processing of germanium under anoxic conditions, and provide an alternative way for studying paleo-redox conditions and biogeochemical processes. Another implication is that Ge and Si might undergo different geologic processes in their global cycles. The study of Ge isotopes, therefore, promises to provide additional constraints on some geological processes. Equilibrium Ge isotope fractionation factors provided in this study will provide a framework for future investigations.

Acknowledgments

We thank the funding support from the Chinese NSF projects (40672033, 40773005, 40803004). Two reviewers—Edwin Schauble and Christine Siebert have provided a lot of valuable and constructive suggestions for us to improve this manuscript. YL thanks Huawen Qi, Hanjie Wen and Olivier Rouxel for inspiring discussions.

Appendix A. Supplementary data

Supplementary data associated with this article can be found, in the online version, at doi:10.1016/j.epsl.2009.07.027.

References

Akesson, R., Pettersson, L.G.M., Sandstroem, M., Siegbahn, P.E.M., Wahlgren, U., 1993. Theoretical study of water-exchange reactions for the divalent ions of the first transition period. J. Phys. Chem. 97, 3765–3774.

Akesson, R., Pettersson, L.G.M., Sandstroem, M., Wahlgren, U., 1994. Theoretical study on water-exchange reactions of the divalent and trivalent metal ions of the first transition period. J. Am. Chem. Soc. 116, 8705–8713.

Anbar, A.D., Jarzecki, A.A., Spiro, T.G., 2005. Theoretical investigation of iron isotope fractionation between $Fe(H_2O)_6^{3+}$ and $Fe(H_2O)_6^{2+}$: implications for iron stable isotope geochemistry. Geochim. Cosmochim. Acta 69, 825–837.

Andersson, M.P., Uvdal, P., 2005. New scale factors for harmonic vibrational frequencies using the B3LYP density functional method with the triple-ζ Basis Set 6-311 + G(d, p). J. Phys. Chem. A 109, 2937–2941.
Bareille, G., Labracherie, M., Mortlock, R.A., Maier-Reimer, E., Froelich, P.N., 1998. A test of $(Ge/Si)_{opal}$ as a paleorecorder of $(Ge/Si)_{seawater}$. Geology 26, 179–182.
Bigeleisen, J., Mayer, M.G., 1947. Calculation of equilibrium constants for isotopic exchange reactions. J. Chem. Phys. 15, 261–267.
Becke, A.D., 1993. Density-functional thermochemistry III. The role of exact exchange. J. Chem. Phys. 98, 5648.
Bernstein, L.R., 1985. Germanium geochemistry and mineralogy. Geochim. Cosmochim. Acta 49, 2409–2422.
Byrne, R.H., Yao, W.S., Klochko, K., Tossel, J.A., Kaufman, A.J., 2006. Experimental evaluation of the isotopic exchange equilibrium $^{10}B(OH)_3 + {}^{11}B(OH)^{-}{}_4 = {}^{11}B(OH)_3 + {}^{10}B(OH)^{-}{}_4$ in acqueous solution. Deep-Sea Res., Part I 53, 684–688.
Cances, E., Mennucci, B., Tomasi, J., 1997. A new integral equation formalism for the polarizable continuum model: theoretical background and applications to isotropic and anisotropic dielectrics. J. Chem. Phys. 107, 3032–3041.
Criss, R.E., 1999. Principles of Stable Isotope Distribution. Oxford University Press, New York. 40–83 pp.
De Argollo, R., Schilling, J.G., 1978. Ge–Si and Ga–Al fractionation in Hawaiian volcanic rocks. Geochim. Cosmochim. Acta 42, 623–630.
De La Rocha, C.L., 2003. Silicon isotope fractionation by marine sponges and the reconstruction of the silicon isotope composition of ancient deep water. Geology 31, 424–426.
Driesner, T., Seward, T.M., 2000. Experimental and simulation study of salt effects and pressure/density effects on oxygen and hydrogen stable isotope liquid–vapor fractionation for 4–5 molal aqueous NaCl and KCl solutions to 400°C. Geochim. Cosmochim. Acta 64, 1773–1784.
Evans, M.J., Derry, L.A., 2002. Quartz control of high germanium/silicon ratios in geothermal waters. Geology 30, 1019–1022.
Fournier, R.O., 1985. The behavior of silica in hydrothermal systems. In: Berger, B.R., Bethke, P.M. (Eds.), Geology and geochemistry of epithermal systems. In: Rev. Econ. Geol., vol. 2. Society of Economic Geologists, pp. 45–62.
Frisch, M.J., Trucks, G.W., Schlegel, H.B., Scuseria, G.E., Robb, M.A., Cheeseman, J.R., et al., 2003. (Revision A.1)[CP]. Gaussian, Inc, Pittsburgh, PA.
Froelich, P.N., Hambrick, G.A., Andrae, M.O., Mortlock, R.A., 1985a. The geochemistry of inorganic germanium in natural waters. J. Geophys. Res. 90, 1133–1141.
Froelich, P.N., Kaul, L.W., Byrd, J.J., Andreae, M.O., Roe, K.K., 1985b. Arsenic, barium, germanium, tin, dimethylsulfide and nutrient biogeochemistry in Charlotte Harbor, Florida, a phosphorus-enriched estuary. Estuar. Coast. Shelf Sci. 20, 239–264.
Froelich, P.N., Blanc, V., Mortlock, R.A., Chillrud, S.N., Dunstan, W., Udomkit, A., Peng, T.H., 1992. River fluxes of dissolved silica to the ocean were higher during glacials: Ge/Si in diatoms, rivers, and oceans. Paleoceanography 7, 739–767.
Galy, A., Pokrovsky, O.S., Shott, J., 2002. Ge-isotopic fractionation during its sorption on goethite: an experimental study. Geochim. Cosmochim. Acta 66, A259.
Gibbs, G.V., 1982. Molecules as models for bonding in silicates. Am. Miner. 67, 421–450.
Goldschmidt, V.M., 1958. Geochemistry. Oxford University Press, Oxford.
Hammond, D.E., Mcmanus, J., Berelson, W.M., Meredith, C., Klinkhammer, G.P., Coale, K.H., 2000. Diagenetic fractionation of Ge and Si in reducing sediments: the missing Ge sink and a possible mechanism to cause glacial/interglacial variations in oceanic Ge/Si. Geochim. Cosmochim. Acta 64, 2453–2465.
Head, J.D., 1997. Computation of vibrational frequencies for adsorbates on surfaces. Int. J. Quantum Chem. 65, 827–838.
Hehre, W.J., Radom, L., Schleyer, P.V.R., Pople, J.A., 1986. *Ab initio* molecular orbital theory. John Wiley and Sons, Inc., New York.
Hildebrand, M., 2000. Silicic Acid Transport and its Control During Cell Wall Silicification in Diatoms. Wiley-VCH, Weinheim. 170–188 pp.
Hildebrand, M., Volcani, B.E., Grassmann, W., Schroeder, J.I., 1997. A gene family of silicon transporters. Nature 385, 688–689.
Holland, H.D., Malinin, S.D., 1979. The Solubility and Occurrence of Nonore Minerals. John Wiley and Sons, Inc, New York. 461–508 pp.
Hu, R.Z., Bi, X.W., Ye, Z.J., Su, W.C., Qi, L., 1996. The genesis of Lincang germanium deposit — a preliminary investigation. Acta Mineral. Sin. 16, 97–102.
Jarzecki, A.A., Anbar, A.D., Spiro, T.G., 2004. DFT analysis of $Fe(H_2O)_6^{3+}$ and $Fe(H_2O)_6^{2+}$ structure and vibrations; implications for isotope fractionation. J. Phys. Chem. A 108, 2726–2732.
Kieffer, S.W., 1982. Thermodynamics and lattice-vibrations of minerals. 5. Applications to phase-equilibria, isotopic fractionation, and high-pressure thermodynamic properties. Rev. Geophys. Space Phys. 20, 827–849.
King, S.L., Froelich, P.N., Jahnke, R.A., 2000. Early diagenesis of germanium in sediments of the Antarctic South Atlantic: in search of the missing Ge sink. Geochim. Cosmochim. Acta 64, 1375–1390.
Klochko, K., Kaufman, A.J., Yao, W., Byrne, R.H., Tossell, J.A., 2006. Experimental measurement of boron isotope fractionation in seawater. Earth Planet. Sci. Lett. 248, 276–285.
Lasaga, A.C., Gibbs, G.V., 1990. Ab-initio quantum mechanical calculations of water–rock interactions: adsorption and hydrolysis reactions. Am. J. Sci. 290, 263.
Lee, C., Yang, W., Parr, R.G., 1988. Development of the Colle–Salvetti correlation-energy formula into a functional of the electron density. Phys. Rev. B 37, 785.
Liu, Y., Nekvasil, H., 2002. Si–F bonding in aluminosilicate glasses — inferences from *ab initio* NMR calculations. Am. Miner. 87, 339–346.
Liu, Y., Long, H.B., Nekvasil, H., 2002. Water dissolution in albite melts: constraints from *ab initio* NMR calculations. Geochimi. Cosmochim. Acta 66, 4149–4163.
Liu, Y., Tossell, J.A., 2003. The possible Al–F bonding in F-bearing aluminosilicate glasses: from *ab initio* ^{19}F NMR calculation study. J. Phys. Chem. B 107, 11280–11289.
Liu, Y., Tossell, J.A., 2005. *Ab initio* molecular orbital calculations for boron isotope fractionations on boric acids and borates. Geochimi. Cosmochimi. Acta 69, 3995–4006.
Luais, B., 2007. Isotopic fractionation of germanium in iron meteorites: significance for nebular condensation, core formation and impact processes. Earth Planet. Sci. Lett. 262, 21–36.
McManus, J., Hammond, D.E., Cummins, K., Klinkhammer, G.P., Berelson, W.M., 2003. Diagenetic Ge–Si fractionation in continental margin environments: further evidence for a non-opal Ge sink. Geochim. Cosmochim. Acta 67, 4545–4557.
Mortlock, R.A., Froelich, P.N., 1987. Continental weathering of germanium: Ge/Si in the global discharge. Geochim. Cosmochim. Acta 51, 2075–2082.
Mortlock, R.A., Charles, C.D., Froelich, P.N., Zibello, M.A., Saltzman, J., Hays, J.D., Burkle, L. H., 1991. Evidence for lower productivity in the Antarctic Ocean during the last glaciation. Nature 351, 220–223.
Murnane, R.J., Stallard, R.F., 1990. Germanium and silicon in rivers of the Orinoco drainage basin. Nature 344, 749–752.
Oi, T., 2000. *Ab initio* molecular orbital calculations of reduced partition function ratios of polyboric acids and polyborate anions. Z. Naturforsch 55a, 623–628.
Oi, T., Yanase, S., 2001. Calculations of reduced partition function ratios of hydrated monoborate anion by the *ab initio* molecular orbital theory. J. Nucl. Sci. Technol. 38, 429–432.
Otake, T., Lasaga, A.C., Watanabe, Y., Ohmoto, H., 2008. Anmalous S isotope fractionations during reactions with an organic surface: I. Theoretical investigations. Geochim. Cosmochim. Acta 72, A712.
Pokrovski, G.S., Schott, J., 1998a. Thermodynamic properties of aqueous Ge(IV) hydroxide complexes from 25 to 350°C: implications for the behavior of germanium and the Ge/Si ratio in hydrothermal fluids. Geochim. Cosmochim. Acta 62, 1631–1642.
Pokrovski, G.S., Schott, J., 1998b. Experimental study of the complexation of silicon and germanium with aqueous organic species: implications for Ge and Si transport and Ge/Si ratio in natural waters. Geochim. Cosmochim. Acta 62, 3413–3428.
Pokrovski, G.S., Martin, F., Hazemann, J.L., Schott, J., 2000. An X-ray absorption fine structure spectroscopy study of germanium–organic ligand complexes in aqueous solution. Chem. Geol. 163, 151–165.
Richet, P., Bottionga, Y., Javoy, M., 1977. Review of hydrogen, carbon, nitrogen, oxygen, sulfur, and chlorine stable isotope fractionation among gaseous molecules. Ann. Rev. Earth Planet. Sci. 5, 65–110.
Rouxel, O., Galy, A., Elderfield, H., 2006. Germanium isotopic variations in igneous rocks and marine sediments. Geochim. Cosmochim. Acta 70, 3387–3400.
Rouxel, O., Escoube, P., Donard, O., 2008. Measurement of Germanium isotope composition in marine samples by hydride generation coupled to MC-ICP-MS. Geochim. Cosmochim. Acta, Suppl. A809.
Rudolph, W.W., Mason, R., Pye, C.C., 2000. Aluminium(III) hydration in aqueous solution. A Raman spectroscopic investigation and an *ab initio* molecular orbital study of aluminium(III) water clusters. Phys. Chem. Chem. Phys. 2, 5030–5040.
Rudolph, W.W., Pye, C.C., 1999. Zinc(II) hydration in aqueous solution. A Raman spectroscopic investigation and an *ab-initio* molecular orbital study. Phys. Chem. Chem. Phys. 1, 4583–4593.
Rustad, J.R., Bylaska, E.J., 2007. *Ab initio* calculation of isotopic fractionation in $B(OH)_3$ (aq) and $B(OH)^{-}_4$(aq). J. Am. Chem. Soc. 129, 2222–2223.
Rustad, J.R., Zarzycki, P., 2008. Calculation of site-specific canbon-isotope fractionation in pidogenic oxide minerals. Proc. Natl. Acad. Sci. U. S. A. 105, 10297–10301.
Rustad, J.R., Nelmes, S.L., Jacksn, V.E., Dixon, D.A., 2008a. Quantum-chemical calculations of carbon-isotope fractionation in CO_2(g), aqueous carbonate species, and carbonate minerals. J. Phys. Chem. A 112, 542–555.
Schauble, E.A., 2004. Applying stable isotope fractionation theory to new systems. Rev. Miner. Geochem. 55, 65–111.
Schauble, E.A., 2007. Role of nuclear volume in driving equilibrium stable isotope fractionation of mercury, thallium, and other very heavy elements. Geochim. Cosmochim. Acta 71, 2170–2189.
Schauble, E.A., Rossman, G.R., Taylor, H.P., 2003. Theoretical estimates of equilibrium chlorine-isotope fractionations. Geochim. Cosmochim. Acta 67, 3267–3281.
Schauble, E.A., Ghosh, P., Eiler, J.M., 2006. Preferential formation of C-13–O-18 bonds in carbonate minerals, estimated using first-principles lattice dynamics. Geochim. Cosmochim. Acta 70, 2510–2529.
Scott, A.P., Radom, L., 1996. Harmonic vibrational frequencies: an evaluation of Hartree–Fock, Moller–Plesset, quadratic configuration interaction, density functional theory and semiempiril scaling factors. J. Phys. Chem. 100, 16502–16513.
Seo, J.H., Lee, S.K., Lee, I., 2007. Quantum chemical calculations of equilibrium copper(I) isotope fractions in ore-forming fluids. Chem. Geol. 243, 225–237.
Sharp, Z., 2005. Principles of Stable Isotope Geochemistry. Pearson Prentice Hall, Upper Saddle River, New Jersey. 22–23 pp.
Shemesh, A., Mortlock, R.A., Froelich, P.N., 1989. Late cenozoic Ge/Si record of marine biogenic opal: implications for variations of riverine fluxes to the ocean. Paleoceanography 4, 221–234.
Siebert, C., Ross, A., McManus, J., 2006. Germanium isotope measurements of high-temperature geothermal fluids using double-spike hydride generation MC-ICP-MS. Geochim. Cosmochim. Acta 70, 3986–3995.
Sumper, M., Brunner, E., 2008. Silica biomineraliation in diatoms: the model organism *Thalassiosira pseudonana*. ChemBioChem 9, 1187–1194.
Tomasi, J., 1994. Thirty years of continuum solvation chemistry: a review, and prospects for the near future. Theor. Chem. Acc. 112, 184–203.
Tossell, J.A., 2005. Calculating the partitioning of the isotopes of Mo between oxidic and sulfidic species in aqueous solution. Geochim. Cosmochim. Acta 69, 2981–2993.
Urey, H.C., 1947. Thermodynamic properties of isotopic substance. J. Chem. Soc. 562–581.
Walrafen, G.E., 1964. Raman spectral studies of alkaline solutions of germanium dioxide. J. Chem. Phys. 42, 485–492.
Zeebe, R.E., 2005. Stable boron isotope fractionation between dissolved $B(OH)_3$ and $B(OH)^{-}_4$. Geochim. Cosmochim. Acta 69, 2753–2766.